Far-Red Fluorescent Protein Excitable with Red Lasers for Flow Cytometry and Superresolution STED Nanoscopy

Kateryna S. Morozova,[†] Kiryl D. Piatkevich,[†] Travis J. Gould,[§] Jinghang Zhang,[‡] Joerg Bewersdorf,[§] and Vladislav V. Verkhusha[†*]

[†]Department of Anatomy and Structural Biology, and Gruss-Lipper Biophotonics Center, and [‡]Flow Cytometry Facility, Albert Einstein College of Medicine, Bronx, New York; and [§]Department of Cell Biology, Yale University School of Medicine, New Haven, Connecticut

ABSTRACT Far-red fluorescent proteins are required for deep-tissue and whole-animal imaging and multicolor labeling in the red wavelength range, as well as probes excitable with standard red lasers in flow cytometry and fluorescence microscopy. Rapidly evolving superresolution microscopy based on the stimulated emission depletion approach also demands genetically encoded monomeric probes to tag intracellular proteins at the molecular level. Based on the monomeric mKate variant, we have developed a far-red TagRFP657 protein with excitation/emission maxima at 611/657 nm. TagRFP657 has several advantages over existing monomeric far-red proteins including higher photostability, better pH stability, lower residual green fluorescence, and greater efficiency of excitation with red lasers. The red-shifted excitation and emission spectra, as compared to other far-red proteins, allows utilizing TagRFP657 in flow cytometry and fluorescence microscopy simultaneously with orange or near-red fluorescence proteins. TagRFP657 is shown to be an efficient protein tag for the superresolution fluorescence imaging using a commercially available stimulated emission depletion microscope.

Received for publication 16 February 2010 and in final form 14 April 2010.

*Correspondence: vladislav.verkhusha@einstein.yu.edu

Far-red fluorescent proteins (FPs) with excitation above 600 nm and emission further than 650 nm are desirable for several reasons. First, they are required for deep-tissue imaging in animals because absorption by hemoglobin drops significantly above 600 nm. Second, far-red FPs can be imaged simultaneously with near-red or orange FPs, which is advantageous for multicolor imaging. Third, because for most FPs excitation efficiency decreases steeply at wavelengths longer than the excitation maxima, only far-red FPs with absorbance maxima above 600 nm can be excited with the standard 633–640-nm red lasers used in flow cytometers, fluorescence-activated cell sorters (FACSs), and laser confocal microscopes. Fourth and last, 635–640 nm is a required excitation line for stimulated emission depletion (STED) imaging (1) with the commercially available TCS STED (Leica, Wetzlar, Germany), a novel superresolution microscope that achieves ~70-nm lateral resolution.

Several monomeric far-red shifted FPs, such as mRaspberry (2), mKate (3), mKate2 (4), mPlum (2), and mNeptune (5) have been described, but their excitation/emission maxima are limited to $\leq$600/650 nm (Table 1). The only available far-red FP with excitation/emission at 611/646 nm, E2-Crimson (extinction coefficient 126,000 M^{-1} cm^{-1}, with a quantum yield 0.23) (6), exists in a tetrameric state, which is incompatible with tagging of individual proteins due to aggregation artifacts. Consequently, use of E2-Crimson in STED microscopy is limited to organelles (6).

To develop a variant with far-red shifted excitation and emission, we used a gene of mKate as a template. We performed several rounds of site-specific and random mutagenesis. After each round, bacterial libraries were screened using FACS followed by selection of the collected clones on petri dishes. Selection criteria were the largest far-red to red fluorescence intensities ratio and brightest emission in the far-red channel. After each round, sequences of the 20–30 best clones were analyzed to remove duplicates and to site-specifically reverse substitutions in the dimerizing interfaces observed previously in the mKate crystal (7). After this step, typically 2–5 clones were used for the next round of random mutagenesis. In cases where several clones contained different mutations at the same position(s), we performed saturated mutagenesis at this position(s) to choose the best mutant. After eight rounds of random mutagenesis we selected the final monomeric variant, named TagRFP657, which contained 10 substitutions compared to the parental mKate, namely K9T, M44Q, K69H, F84W, S148H, S165T, D166A, M167L, L181F, and R203Y (numbering follows the alignment with common EGFP, see Fig. S1 in the Supporting Material).

From the purified TagRFP657 protein, we determined absorbance/excitation spectra with maxima at 611 nm and fluorescence emission spectrum with a maximum at 657 nm (Fig. 1 *A*). Its extinction coefficient and quantum yield were measured to be 34,000 M^{-1} cm^{-1} and 0.10, respectively, and are comparable to those of other far-red FPs (Table 1). Because a substantially enhanced variant of mKate called mKate2 was published (4) during completion of the TagRFP657 development, we further compared TagRFP657

Editor: Petra Schwille.

doi: 10.1016/j.bpj.2010.04.025

TABLE 1 Properties of TagRFP657 in comparison with other monomeric far-red FPs with fluorescence emission above 625 nm

Protein	Excitation/ emission peaks (nm)	QY	EC (M^{-1} cm^{-1})	BR relative to mKate2 (%)	EC at 633 nm (M^{-1} cm^{-1})	BR with 633-nm excitation above 650 nm (%)	p*K*a	Bleaching half-time (s)	Maturation half-time at 37°C (min)
mRaspberry	598/625	(0.15)*	(79,000)*	(47)*	6700	130	(5.0) †	ND	(126) †
		(0.14) †	(42,000) †	(24) †	3600	69			
mKate	588/635	(0.28) ‡	(31,500) ‡	(35) ‡	1300	36	(6.5)*	ND	(75)*
mKate2	588/633	(0.40) ‡	(62,500) ‡	(100) ‡	2600	100	(6.5) †	25	(48) †
		(0.39) †	(56,400) †	(88) †	2300	88	6.5		50
mPlum	590/649	(0.10)*	(22,000)*	(9)*	1700	7.6	(5.5) †	ND	(96) †
		(0.10) †	(29,300) †	(12) †	2300	10			
mNeptune	600/650	(0.20) §	(67,000) §	(54) §	11,400	280	(5.4) §	13	ND
		0.20	59,000	47	10,000	240	5.7		
TagRFP657	611/657	0.10	34,000	14	17,000	250	5.0	55	125

Data available from other articles are presented in parentheses. Other parameters were determined using the same conditions as for TagRFP657 (see Supporting Material). Brightness (BR) is a product of excitation coefficient (EC) and quantum yield (QY). Photobleaching half-times are indicated for 47.1 mW/cm^2 intensity at the back focal plane of a 100× oil objective lens. ND, not determined.

* Shcherbo et al., 2007 (3).

† Strack et al., 2009 (6).

‡ Shcherbo et al., 2009 (4).

§ Lin et al., 2009 (5).

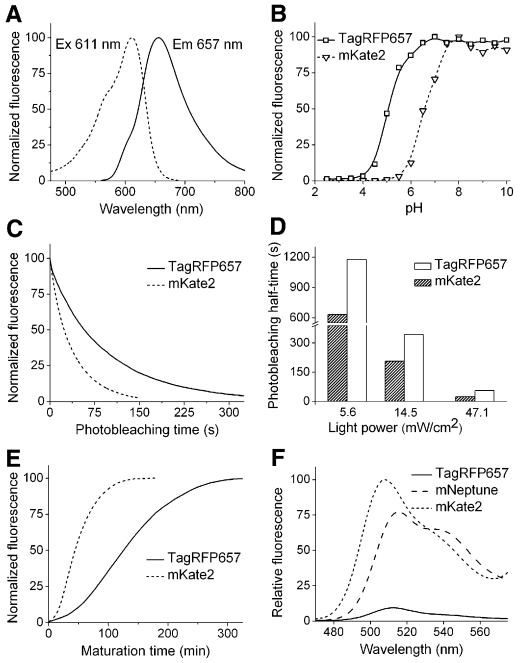

FIGURE 1 TagRFP657 properties. (*A*) Excitation (*dashed line*) and emission (*solid line*) spectra. (*B*) Equilibrium pH dependence for TagRFP657 (*solid line*) and mKate2 (*dashed line*). (*C*) Photobleaching kinetics of TagRFP657 (*solid line*) and mKate2 (*dashed line*) at 47.1 mW/cm^2. (*D*) Photobleaching half-times for TagRFP657 (*open columns*) and mKate2 (*dashed columns*) at different light intensities. Intensities were measured at the back-focal plane of a 100× oil objective. Photobleaching data were normalized to spectral output of the lamp, transmission profiles of the filter and dichroic mirror, and FP absorbance spectra. (*E*) Maturation kinetics of TagRFP657 (*solid line*) and mKate2 (*dashed line*) at 37°C. (*F*) Residual green fluorescence of TagRFP657 (*solid line*), mKate2 (*dashed line*), and mNeptune (*long dashed line*) when excited at 460 nm. Relative areas under the emission spectra in the 470–570-nm range were 100% (mKate2), 83% (mNeptune), and 8% (TagRFP657).

to mKate2. Fluorescence of TagRFP657 had higher pH stability than mKate2 (Fig. 1 *B*) with an apparent pK_a value of 5.0. The high pH stability of TagRFP657 will allow its imaging in acidic intracellular compartments, such as endosomes and lysosomes, exhibiting pH values as low as 5.2. At a high intensity of the wide-field photobleaching light (47.1 mW/cm^2), TagRFP657 photobleached 2.2-fold slower than mKate2 (Fig. 1 *C*). The difference in the photostability slightly reduced with decreasing intensity level (Fig. 1 *D*). At the lowest tested intensity of 5.6 mW/cm^2, TagRFP657 was 1.8-fold more photostable than mKate2. The 125-min chromophore maturation half-time of TagRFP657 was slower than that of mKate2 (Fig. 1 *E*). On the other hand, the TagRFP657 maturation was more efficient than that of mKate2 and recently published mNeptune (5), as indicated by the substantially lower residual green fluorescence (Fig. 1 *F*), which corresponds to a dead-end product of the chromophore formation (8). TagRFP657 behaved as a monomer both in the purified state (Fig. S2) and when expressed in six fusion constructs in living cells (Fig. S3).

The shifts of both the excitation and emission maxima of TagRFP657 made it almost undetectable with the standard red filter sets for red FPs (Fig. S2 *B*). We characterized the fluorescence brightness above 650 nm at 633-nm excitation as a criterion for practical application with a common red HeNe laser (3,4,6). TagRFP657 was 2.5-fold brighter than mKate2 and had the same brightness as mNeptune (Table 1). The sharp decrease of most FP excitation spectra at wavelengths longer than the excitation maxima explains why TagRFP657 excites at 633 nm with 50% efficiency whereas the spectrally closest FP, mNeptune, excites with 17% (threefold lower) efficiency only (Table 1).

To demonstrate the application of strong TagRFP657 excitation with standard red lasers and its suitability for labeling experiments with three red colors, we mixed cells

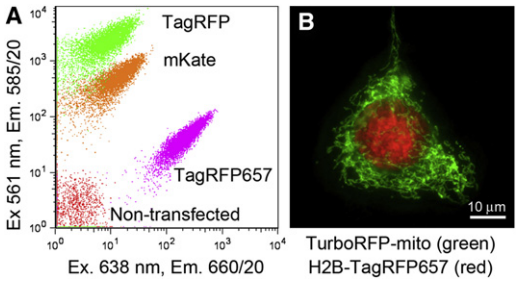

FIGURE 2 Simultaneous detection of several red FPs expressed in live mammalian cells. (*A*) Using flow cytometry: sorting of a mixture of TagRFP657, mKate, and TagRFP expressing as well as nontransfected cells. (*B*) Using wide-field fluorescence microscopy: coexpression of histone-2B (H2B) tagged TagRFP657 and TurboRFP targeted to mitochondria. (Note that all colors used in this figure are pseudocolors.)

transfected with different red FPs, namely TagRFP (9) (excitation, 555 nm; emission, 584 nm), mKate and TagRFP657, and applied them to FACS equipped with solid-state 561-nm and 638-nm lasers (Fig. 2 *A*). The TagRFP657 cell population was easily separable from the other cell populations. The TagRFP657 cells were ~10-fold brighter in the 638-nm channel than mKate, which is consistent with the measurements of the purified proteins (Table 1). Furthermore, fusion constructs with TagRFP657 and a dimeric variant of TagRFP, TurboRFP (9), coexpressed in the same cells were fully spectrally resolvable using a wide-field microscope with standard filter sets (Fig. 2 *B* and Fig. S4).

Its red-shifted excitation spectrum makes TagRFP657 the only monomeric FP applicable for the commercial STED microscope, which utilizes a 635–640-nm laser for fluorescence excitation and 750-nm laser line for emission depletion. For STED imaging, we fused TagRFP657 with a microtubule-associating factor EB3 and imaged transfected HeLa cells using standard confocal and STED microscopy (Fig. 3). Imaged microtubules exhibit threefold better resolution in the STED than in the confocal image (Fig. 3, *E* and *F*). The obtained 74-nm full width at half-maximum is close to the theoretically achievable instrument resolution (10) and does not reflect TagRFP657 limitations. Confocal and STED images of cells expressing α-actinin, histone-2B, EGF receptor, and mitochondria tagged with TagRFP657 are shown in Fig. S5, Fig. S6, Fig. S7, and Fig. S8, respectively.

SUPPORTING MATERIAL

Eight figures and full materials and methods are available at http://www.biophysj.org/biophysj/supplemental/S0006-3495(10)00522-9.

ACKNOWLEDGMENTS

This work was supported by National Institutes of Health grant R01 GM073913 to V.V.V..

REFERENCES and FOOTNOTES

1. Hell, S. W. 2009. Microscopy and its focal switch. *Nat. Methods*. 6:24–32.

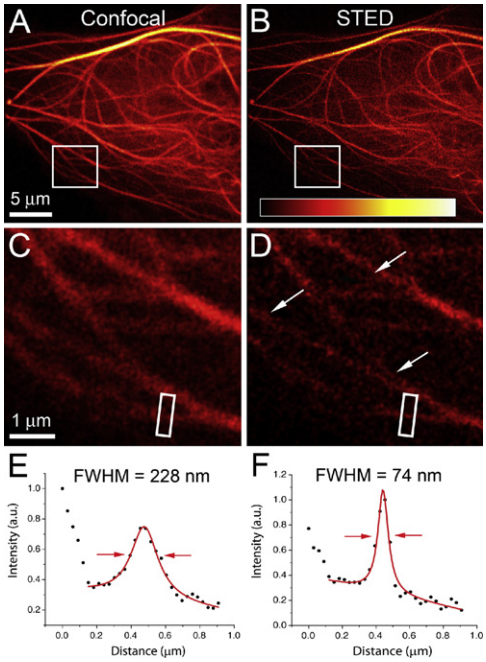

FIGURE 3 Imaging of EB3-TagRFP657 fusion in mammalian cells using (*A*) standard confocal and (*B*) superresolution STED microscopy. Magnified views of the square areas in panels *A* and *B* are shown for confocal (*C*) and STED (*D*) images. Profiles displayed in panels *E* and *F* were generated from identical regions of interest shown in panels *C* and *D*. Uncolored arrows indicate details only resolvable in STED (*D*). The profiles were measured along the longer side of the regions of interest, averaging over the shorter side. Solid red lines in panels *E* and *F* indicate the Gaussian (confocal) and Lorentzian (STED) fits used to determine the displayed full width at half-maximum values (illustrated with *red arrows*). Image color-maps were scaled to minimum and maximum values in panels *A* and *B*.

2. Wang, L., W. C. Jackson, …, R. Y. Tsien. 2004. Evolution of new nonantibody proteins via iterative somatic hypermutation. *Proc. Natl. Acad. Sci. USA*. 101:16745–16749.

3. Shcherbo, D., E. M. Merzlyak, …, D. M. Chudakov. 2007. Bright far-red fluorescent protein for whole-body imaging. *Nat. Methods*. 4:741–746.

4. Shcherbo, D., C. S. Murphy, …, D. M. Chudakov. 2009. Far-red fluorescent tags for protein imaging in living tissues. *Biochem. J*. 418: 567–574.

5. Lin, M. Z., M. R. McKeown, …, R. Y. Tsien. 2009. Autofluorescent proteins with excitation in the optical window for intravital imaging in mammals. *Chem. Biol*. 16:1169–1179.

6. Strack, R. L., B. Hein, …, B. S. Glick. 2009. A rapidly maturing far-red derivative of DsRed-Express2 for whole-cell labeling. *Biochemistry*. 48:8279–8281.

7. Pletnev, S., D. Shcherbo, …, V. Pletnev. 2008. A crystallographic study of bright far-red fluorescent protein mKate reveals pH-induced *cis-trans* isomerization of the chromophore. *J. Biol. Chem*. 283:28980–28987.

8. Verkhusha, V. V., D. M. Chudakov, …, K. A. Lukyanov. 2004. Common pathway for the red chromophore formation in fluorescent proteins and chromoproteins. *Chem. Biol*. 11:845–854.

9. Merzlyak, E. M., J. Goedhart, …, D. M. Chudakov. 2007. Bright monomeric red fluorescent protein with an extended fluorescence lifetime. *Nat. Methods*. 4:555–557.

10. Fitzpatrick, J. A. J., …, Q. Yan, M. P. Bruchez. 2009. STED nanoscopy in living cells using fluorogen activating proteins. *Bioconjug. Chem*. 20:1843–1847.